

VIIRS polarization sensitivity testing and analysis

Eric C. Fest*

Raytheon Company, 1151 E. Hermans Road, MS 840/4, Tucson, AZ, USA 85756-9367

ABSTRACT

A requirement for the Visible/Infrared Imager Radiometer Suite (VIIRS) is that its polarization sensitivity be 3% or less for all VISNIR bands (412-865 nm). A test using a rotating polarizer sheet was performed on the sensor to validate this requirement, and though the test results show that the requirement is met, they also show a large variation in this polarization sensitivity (as much as 2%) across the field of view (FOV) in track. Though this result is unexpected, it may be the result of natural variations in the diattenuation and retardance of the VIIRS optics as a function of field angle. To test this theory, a raytracing model of the system was constructed using measured ellipsometric data from the VIIRS optics, and the polarization sensitivity of the model was computed. Using the nominal ellipsometric data, good correlation between the predicted and measured polarization sensitivity was not achieved. However, by applying small variations to the ellipsometric data as a function of position on the optics, it was possible to achieve good correlation. This paper gives the details of the sensor polarization sensitivity measurements, ellipsometric measurements, and raytracing analysis.

Keywords: VIIRS, NPOESS, polarization sensitivity, ellipsometry, FSS-99-500, remote sensing, radiometry

1. INTRODUCTION

VIIRS is a remote-sensing system that is a part of the National Polar-orbiting Operational Environmental Satellite System (NPOESS). VIIRS is a “whisk-broom” type scanning system, and has very strict requirements for radiometric accuracy. Because the atmosphere can linearly polarize ground-leaving radiance¹, it is important to minimize the sensor’s polarization sensitivity so that the radiometric accuracy requirement can be met. Polarization sensitivity quantifies the variation in sensor response as a function of incident polarization state, and is defined as

$$\frac{\Phi_{\max} - \Phi_{\min}}{\Phi_{\max} + \Phi_{\min}} \quad (1)$$

where Φ_{\max} is the flux at the detector (in Watts) resulting from the input polarization state with maximum transmittance, and Φ_{\min} is the flux corresponding to the polarization state with minimum transmittance. The VIIRS polarization sensitivity requirement is defined in terms of sensitivity to the orientation of linear polarization only, and therefore there is no requirement for sensitivity to elliptical polarization. It can be shown² that the polarization sensitivity defined in Eq. (1) is equal to the Degree of Linear Polarization (DoLP) of the beam at the detector, which quantifies the percentage of the beam flux that is linearly polarized. The polarization sensitivity requirements for VIIRS are specified in Table 1.

This paper will discuss the optical design of the VIIRS sensor and the initial polarization raytracing model of the system. The details of the sensor-level polarization test will be discussed, and the results of the sensor test will be compared with the predictions made by the polarization model. In addition, the changes made to the polarization model to achieve better correlation between the predicted and measured results will also be discussed.

1.1 VIIRS Optical Design

The VIIRS optical system is $f/6.15$ and has an entrance pupil diameter of 7.3 inches, and is shown in Figure 1. It consists of a Rotating Telescope Assembly (RTA), followed by a fold mirror and a de-rotation mirror (also called the Half-Angle Mirror or HAM). The RTA is an afocal three-mirror anastigmat, and rotates about the axis shown in Figure 1. The HAM is followed by another fold mirror which is at a compound rotation angle (i.e. it has both an alpha and a beta tilt) relative to the other optical elements. This fold mirror is followed by the Aft-Optics Assembly (AOA), which is an off-axis four-

* eric@raytheon.com; phone (520) 545-7701; fax (520) 794-0872

mirror anastigmat. After the AOA is a dichroic beamsplitter (DBS1) which is used to reflect the visible-to-near-infrared (VISNIR, 412-865 nm) wavebands to VISNIR Focal Plane Assembly (FPA). Polarization sensitivity requirements are defined only for the VISNIR bands, and therefore this analysis will not consider the IR bands. Between DBS1 and the silicon VISNIR Focal Plane Assembly (FPA) is an Integrated Filter Assembly (IFA) which contains the bandpass filters for each of the VISNIR bands (M1-M7, I1-I2).

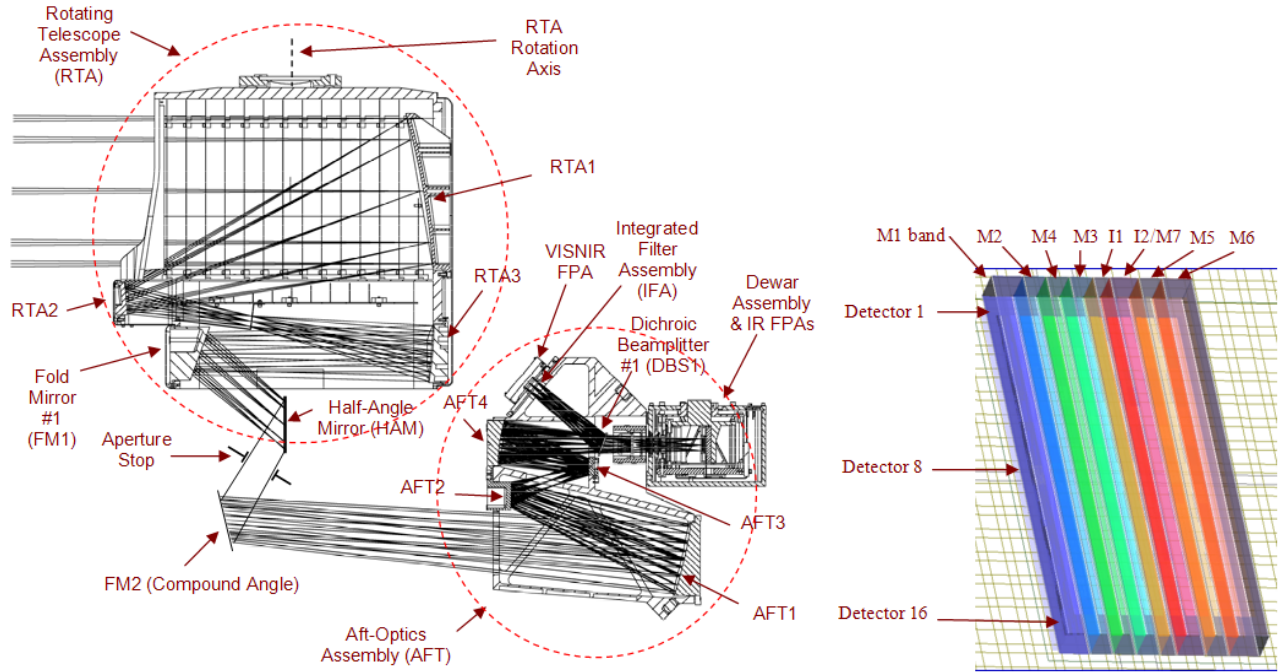


Figure 1. The VIIRS optical system (left) and detail of the VISNIR IFA and detector plane (right).

Table 1. Maximum allowed polarization sensitivity (DoLP) for each band. These requirements are for scan angles 45° or less from NADIR.

Band	Center λ , nm (Bandwidth λ)	Maximum Polarization Sensitivity
M1	412 (20)	3%
M2	445 (18)	2.5%
M3	488 (20)	2.5%
M4	555 (20)	2.5%
I1	640 (80)	2.5%
M5	672 (20)	2.5%
M6	746 (15)	2.5%
M7	865 (39)	3%
I2	865 (39)	3%

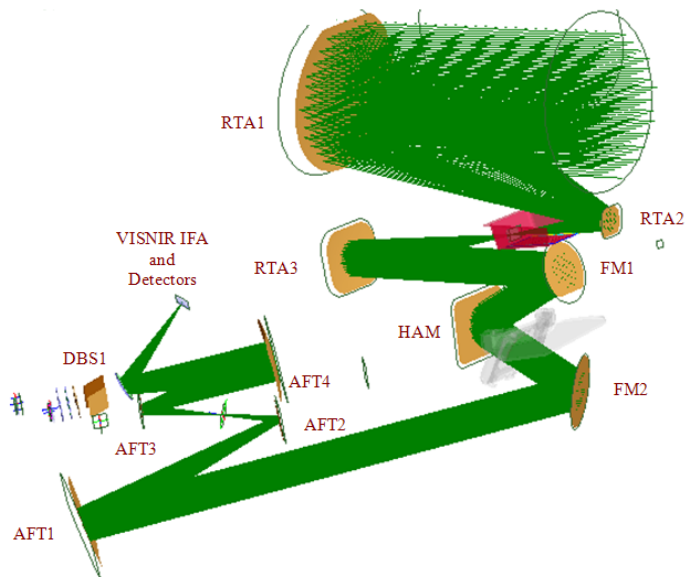


Figure 2. The FRED optical raytracing model of the VIIRS optical system.

Each band consists of a linear along-track array of either 16 detectors (for the M bands) or 32 detectors (for the I bands). The layout of the VISNIR IFA and detectors is shown in Figure 1. All mirrors are coated the “FSS-99-500” coating, which is a proprietary space-qualified protected-silver coating³.

Requirements for the maximum allowed diattenuation D of each optical element ($D=(R_s-R_p)/(R_s+R_p)$ for reflective elements, where R_s and R_p are s and p polarized reflectance, respectively) were derived from the sensor polarization sensitivity requirement. The manufacturers of the optical elements were required to demonstrate compliance to these requirements using ellipsometric measurements. It should be noted that these measurements were performed on flat witness samples and not on the optical elements themselves, since ellipsometric measurements on curved optics are very difficult.

2. METHODOLOGY

2.1 Polarization raytracing model

A model of the VIIRS optical system was constructed in the FRED optical analysis program, and is shown in Figure 2. This model includes all of the optical surfaces of the VISNIR path, and allows the RTA and HAM to be rotated so different scan mirror configurations can be simulated. The polarization raytracing calculations in FRED were checked against two other widely-used optical analysis programs, CODE V and ZEMAX, and the results were nearly identical. The geometry of this model is identical to the geometry analyzed in a previous estimate of the polarization sensitivity⁴, however, the reflectance and transmittance data used is different (the previous model did not incorporate ellipsometric measurements of the mirror coatings).

The s and p polarized reflectance (R_s , R_p), s and p polarized transmittance (T_s , T_p), and retardance (Δ) of each element in the system are modeled using a combination of theoretical and measured data. The theoretical data consists of tables of R_s , R_p , and Δ given as a function of wavelength and Angle Of Incidence (AOI). These tables were generated using the thin-film stack definitions of the mirror coatings, DBS1 coating, IFA coatings, and detector substrate coating, and were generated at high spectral and angular resolution (typically 1 nm and 5°, respectively), therefore, there should be little error as the result of interpolation (which is linear in FRED) between defined wavelength and AOIs. The model uses 121 rays in the pupil and one wavelength per band, and the maximum error associated with this finite sampling was determined to be 0.5% in DoLP.

To increase the accuracy of these predictions, correction factors were applied to these data using ellipsometric measurements of mirror witness samples and spare parts. Ideally, measurements would be performed on the samples and spares at all applicable wavelengths and AOIs, since measured data is usually more accurate than predicted. However, the minimum AOI that most ellipsometers can measure is usually larger than the minimum AOI used by the VIIRS elements. For instance, the V-VASE ellipsometer (a widely-used ellipsometer made by J. A. Woollam Co., Inc.) has a minimum AOI of about 25 degrees. However, the minimum AOI used by most of the VIIRS optical elements is much less than this, as shown in Table 2. Therefore, it is not possible to obtain ellipsometric measurements of the samples and spares at the full range of AOIs the elements are used at. However, it is possible to use these measurements to compute a correction factor $F(\text{AOI})$ that can be applied to the thin-film predictions. Values of F for different AOIs are given in Table 3. F scales R_s such that its value at AOI=0° is determined entirely by the thin-film prediction and its value at AOI=25° is determined entirely by the measured value. In this way, the measured data is used to increase the accuracy of the reflectance model. In all cases, $|F(\text{AOI})-1|<0.01$. In cases where AOI>25° (such as on the HAM) the measured data is used without a correction factor.

Table 2 also specifies the manufacturer of each optical element and the part used in its ellipsometric measurements. Regardless of their manufacturer, all mirrors were coated by Denton Vacuum, Inc. (now Quantum Coatings, Inc.) using their proprietary “FSS-99-500” coating. The prescription of this coating is proprietary to Denton and is not known to Raytheon. The ellipsometric measurements were performed by J. A. Woollam Co., Inc., using their V-VASE ellipsometer. Some measurements at Woollam were repeated in order to determine their accuracy, which was found to be $\pm 0.15\%$ in diattenuation and $\pm 1^\circ$ in retardance, which is within their stated accuracy. Measurements were not performed on the IFA and VISNIR detector substrate, so in these cases only thin-film predictions are used. Plots of some of the data used to model the reflectance and retardance of the VIIRS optics are shown in Figures 3-6. s and p transmittance and retardance data for the IFA and detector substrate are not shown because the diattenuation and retardance of these elements are very nearly equal to 1 and 0, respectively, since these elements are illuminated at nearly normal incidence. FRED uses the Abeles⁵ convention for retardance in which the retardance of a beam reflected at AOI=0° is 0°.

In general, the biggest source of error in the polarization raytracing model is the probably the lack of measured ellipsometric data at AOIs less than 25°. The inability to measure the ellipsometric parameters and their variation over the apertures of the actual optical elements may also be a factor.

Table 2. Details of the reflectance and retardance data used in the VIIRS model. The AOI on the HAM mirror varies as a function of scan angle from 54° to 27° for scan angles from -45° to +45° (relative to NADIR)

Element	Manufacturer	Used AOIs			Sample measured by J. A. Woollam
		Min	Avg	Max	
RTA1	Axsys	6.2	10.5	14.9	RTA witness
RTA2	Axsys	9.4	15.6	22.5	RTA witness
RTA3	Axsys	2.8	4.9	6.8	RTA witness
FM1	Axsys	13.2	13.2	13.2	RTA witness
HAM	Axsys	39.5	39.5	39.5	Spare HAM
FM2	MRC	24.5	24.5	24.5	Spare FM2
AFT1	ELCAN	5.6	7.3	8.7	AFT witness
AFT2	ELCAN	13.2	17.7	19.5	AFT witness
AFT3	ELCAN	9.5	13.7	18.1	AFT witness
AFT4	ELCAN	4.3	5.8	5.9	AFT witness
DBS1	OCLI/JDSU	17.5	24.7	26.9	DBS1 spare
IFA	Barr	0.3	6.7	12.9	N/A (not measured)
Detector	Raytheon Vision Systems	0.1	1.5	2.5	N/A (not measured)

Table 3. Correction factor (F) values for various AOIs.

AOI (°)	F
0	1
0 < AOI < 25	Linearly interpolated between 1 and F(25)
25	R_s (measured) / R_s (predicted)

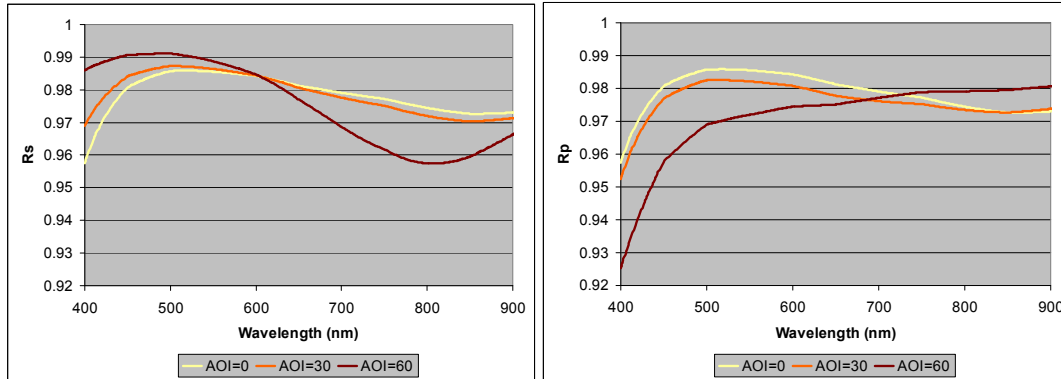


Figure 3. s and p reflectance of the FSS-99-500 protected silver coating thin-film model from Denton Vacuum.

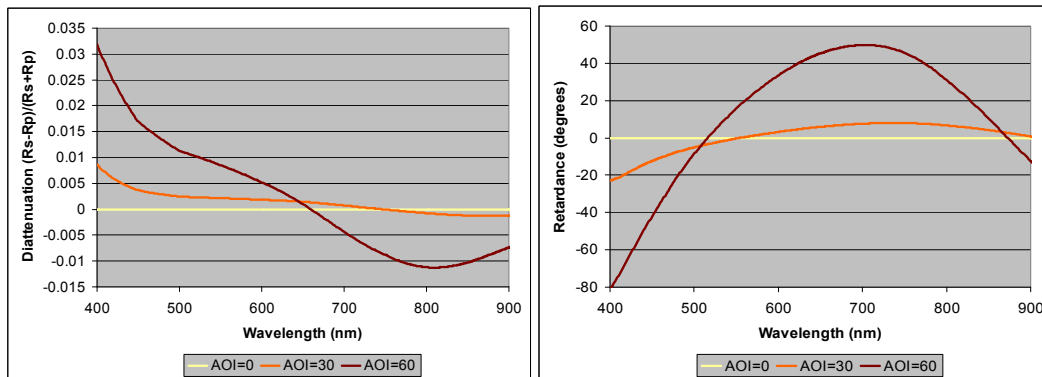


Figure 4. Diattenuation (left) and retardance (right) of the FSS-99-500 protected silver coating model from Denton Vacuum.

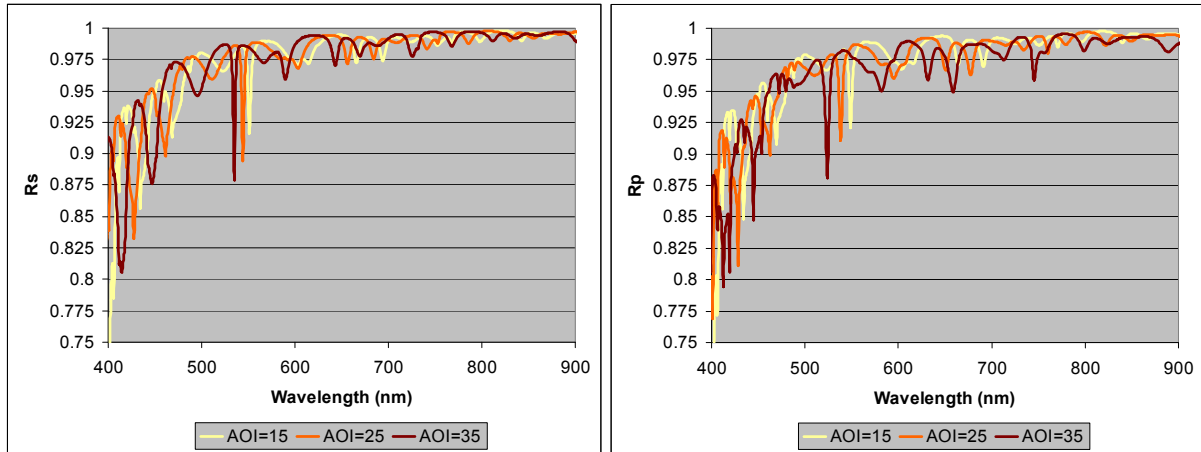


Figure 5. s and p reflectance of the dichroic beamsplitter 1 (DBS1) thin-film coating model from OCLI.

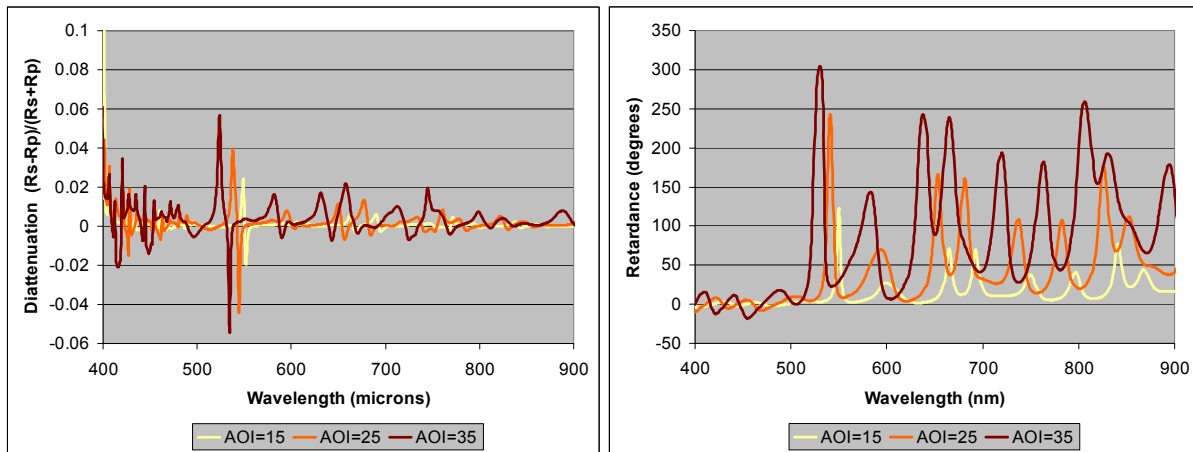


Figure 6. Diattenuation and retardance of the dichroic beamsplitter 1 (DBS1) thin-film coating model from OCLI.

2.2 Expected characteristics of the VIIRS polarization sensitivity

Some characteristics of the VIIRS polarization sensitivity can be determined from the asymmetry of its optical design and the diattenuation and retardance of its optical components. These characteristics can be determined independently of the raytracing model, and can thus be used to validate the model results:

- The polarization sensitivity will be asymmetric across the field (e.g. with respect to the VISNIR band or along-track detector number). This is because most optical elements in the system have off-axis apertures, and the footprints of the ray bundles for each of the VISNIR detectors do not lie symmetrically on each of the optical elements, as shown in Figure 7 for the AFT1 mirror. Therefore, the collection of AOIs of each element for each band/detector combination is different and will result in an asymmetric polarization response with field.
- The polarization sensitivity will be asymmetric across the range of scan mirror angles. This is because the AOI on the HAM is 54° at scan angle $= -45^\circ$ and 27° at scan angle $= +45^\circ$, and thus is not change symmetrically over scan.

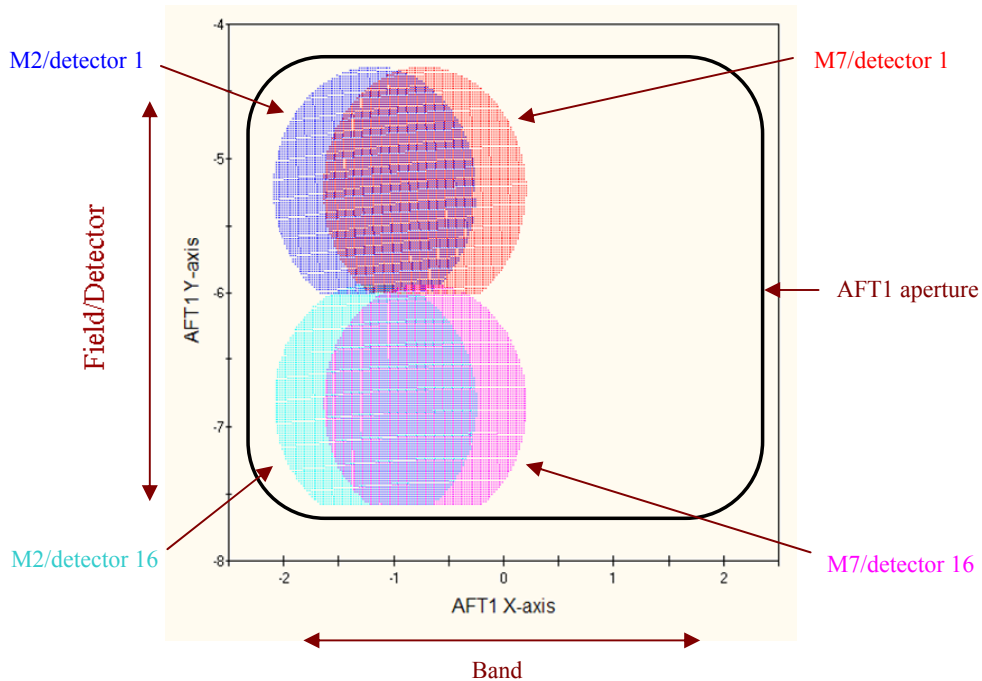


Figure 7. Ray bundle footprints on the AFT1 mirror for bands M1 and M7, detectors 1 and 16. The x and y axis values are with respect to the vertex of the mirror radius of curvature. The VIIRS aperture stop is “D” shaped, and therefore the footprints are not circular.

- The polarization sensitivity will be asymmetric across the pupil. This is because the plane of incidence is rotated upon reflection from the HAM and FM2. The plane of incidence remains relatively fixed as the beam moves through the RTA and FM1, but because the reflection from the HAM occurs at a compound angle, the plane of incidence (and thus the orientation of the s and p vectors) is rotated relative the plane of incidence defined by the RTA. This rotation angle varies from about 57° at scan angle $=-45^\circ$ from NADIR to about 3° at scan angle $=+45^\circ$. Then the plane of incidence is rotated again by FM2, this time by an even larger angle (117° at scan angle $=-45^\circ$, 57° at scan angle $=+45^\circ$). This means that the HAM and FM2 can act as compensators for the polarization sensitivity induced by the other elements in the system. The plane of incidence then remains relatively fixed as the beam moves through the AFT optics, DBS1, and the IFA.

Thus, the polarization sensitivity is asymmetric across the field, scan angle, and pupil, and therefore the raytracing results should be asymmetric as well.

The diattenuation and retardance of the sensor optical components also suggest the following characteristics of the polarization sensitivity:

- Figure 4 shows that the diattenuation of the FSS-99-500 mirror coating is very low at wavelengths near 650 nm. This suggests that the polarization sensitivity of the M5 band ($\lambda=672$ nm) will be a weak function of the mirror diattenuation.
- The variation in polarization sensitivity vs. scan angle will be complicated: the AOI is higher on the HAM at more negative scan angles (54° at scan angle $=-45^\circ$ and 27° at scan angle $=+45^\circ$), so the diattenuation and retardance of the HAM is higher at these angles. Diattenuation will increase the polarization sensitivity, but retardance can either increase or decrease sensitivity, depending on how the retardance effects the compensation of polarization sensitivity from elements after the HAM.
- The variation in polarization across the field for any particular band will be a strong function of spatial variations in diattenuation and retardance across the AFT1, AFT2, and AFT3 mirrors, since the beam footprint undergoes a large shift in position with field angle for these elements, as shown in Figure 7 for AFT1.

2.3 Sensor polarization sensitivity test

The polarization sensitivity of the VIIRS Flight Unit 1 (F1) sensor was tested using the equipment illustrated in Figure 8. The sensor looks through a rotating linear polarizer at a Spherical Integrating Sphere (SIS), and the modulation of the output signal that results from the polarizer rotation is compared to the requirements in Table 1. To quantify the effect of scan mirror rotation on the polarization sensitivity, this test is performed at multiple angles of the RTA. Discussion of the test equipment calibration and procedure are beyond the scope of this paper, and therefore the assumption will be made that the results of the polarization sensitivity test are accurate to within 0.5% uncertainty in DoLP. Results for the M1 band have higher uncertainty and therefore will not be shown.

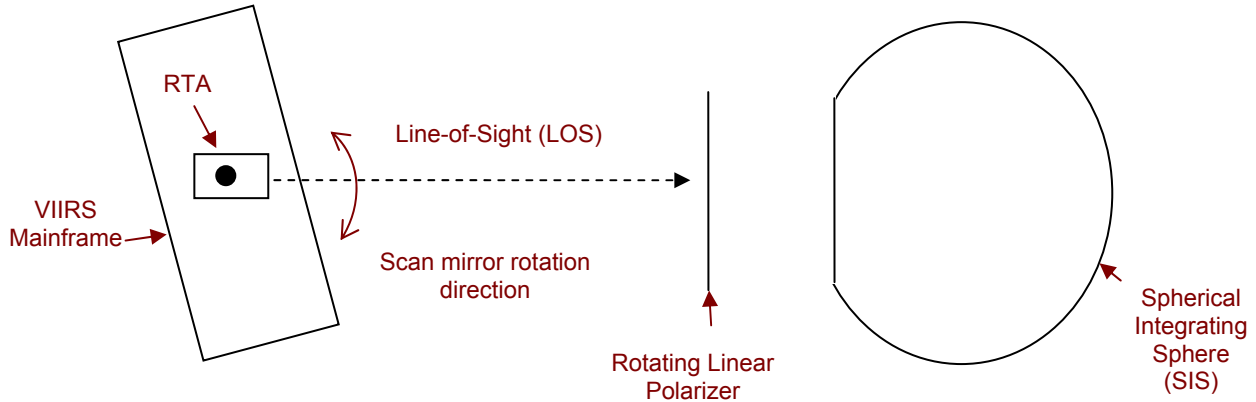


Figure 8. Schematic of VIIRS polarization sensitivity test.

3. DATA

3.1 Polarization raytracing model and sensor test results

The predicted and measured DoLP for each band are shown in Figures 9 – 12 for scan angles (SA) -45° , -8° , and $+45^\circ$. The performance of I bands are not shown. As expected, there is no symmetry in the polarization response with field or scan angle, and for many bands the polarization sensitivity is highest at scan angle $=-45^\circ$. Figure 13 shows the predicted polarization sensitivity of the sensor as a function of pupil position as the beam passes through the system. As expected, the polarization sensitivity at the detector shows no symmetry with respect to pupil position, and the HAM and FM2 act as compensators to the polarization sensitivity induced by the RTA mirrors and FM1. A similar plot for band M5 band shows that the polarization sensitivity is weakly dependent on mirror diattenuation. For bands such as M1 and M2, the higher retardance of the HAM at more negative scan angles results in lower polarization sensitivity due to increased compensation by the elements after the HAM, whereas for band M5 the increased diattenuation of the HAM at more negative scan angles results in higher polarization sensitivity. Except for the predicted results for M1, scan angle $=-45^\circ$, all predictions and measurements show that the sensor is compliant to the requirements given in Table 1.

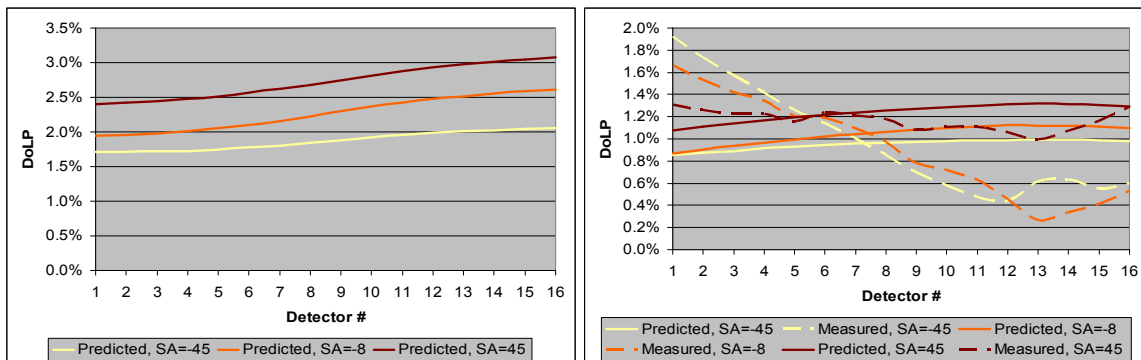


Figure 9. Band M1 (left) and M2 (left) nominal predicted and measured linear polarization sensitivity (DoLP).

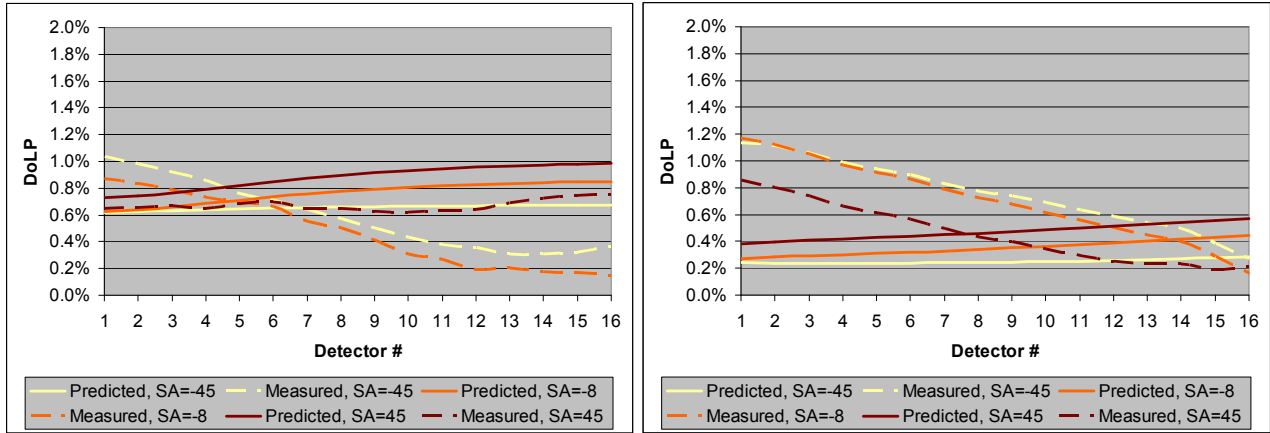


Figure 10. Band M3 (left) and M4 (right) nominal predicted and measured linear polarization sensitivity (DoLP).

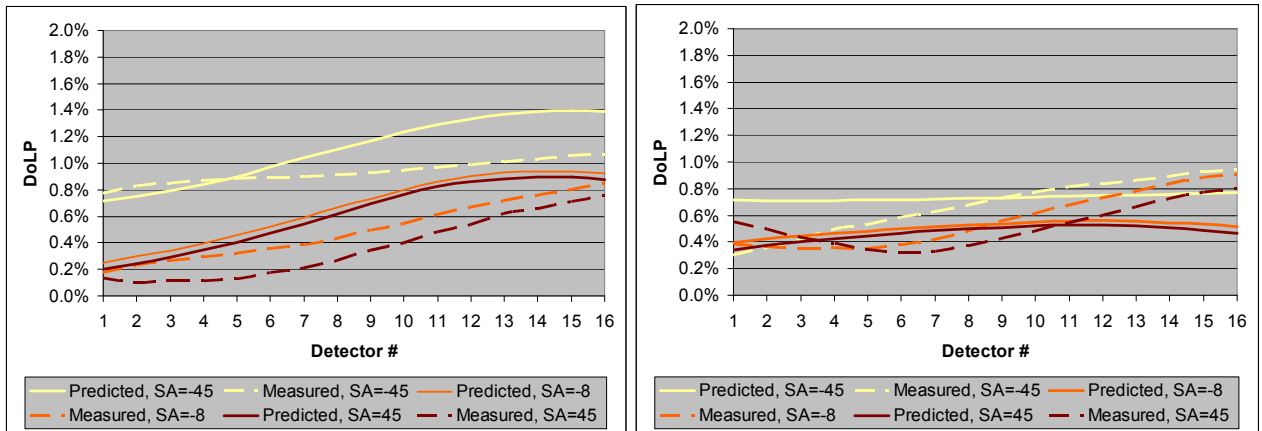


Figure 11. Band M5 (left) and M6 (right) nominal predicted and measured linear polarization sensitivity (DoLP)

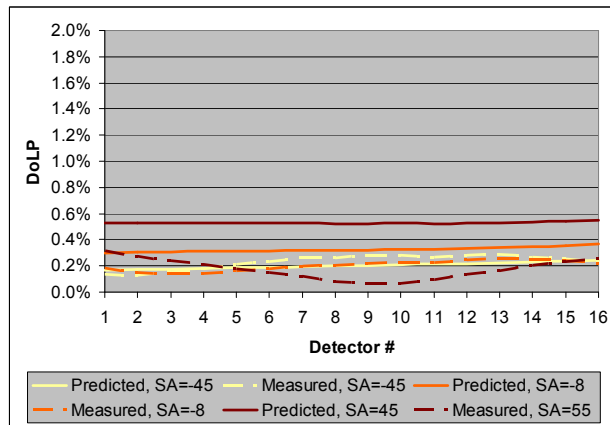


Figure 12. Band M7 nominal predicted and measured linear polarization sensitivity (DoLP)

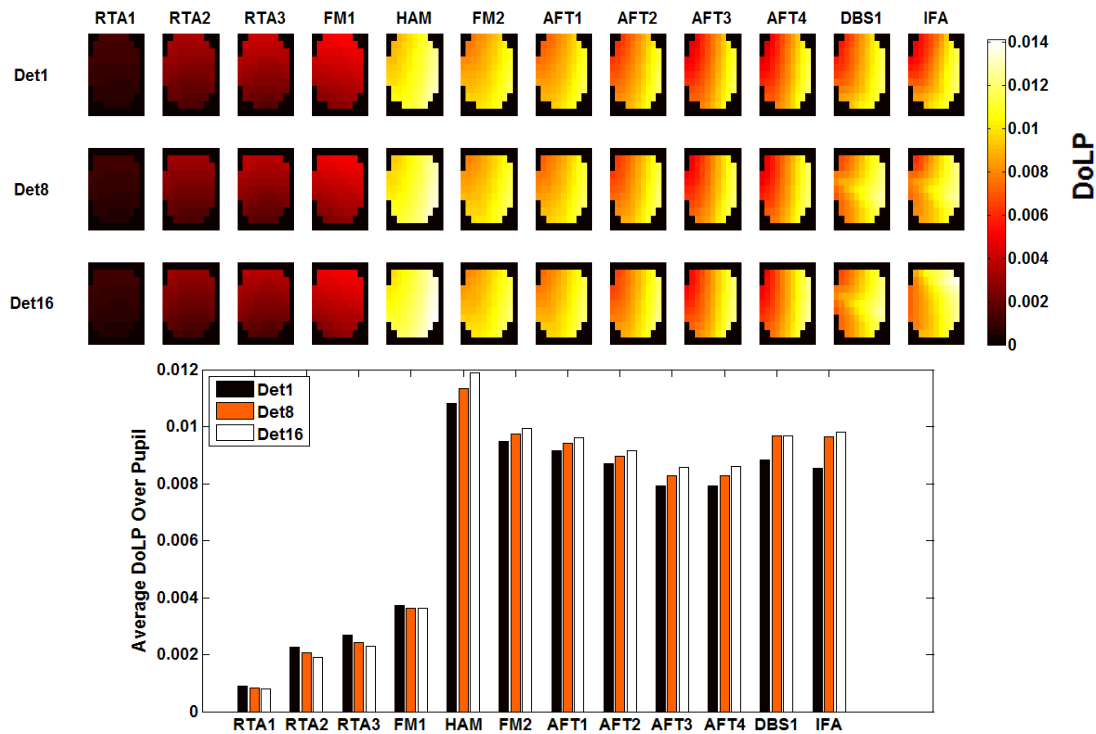


Figure 13. Nominal predicted DoLP vs. pupil position and detector # for band M2, scan angle=-45 (top) and the pupil-averaged DoLP for the same (bottom). The pupil-averaged results for the IFA show the same variation in DoLP vs. detector number as Figure 9.

In general, the difference in DoLP between the prediction and the measurement decreases with wavelength, and can differ by as much as 1.2% at the M2 wavelength (445 nm). In particular, the prediction underestimates the variation in field. This suggests that there is a variation in the diattenuation and/or retardance of the optical elements as a function of position that is not accounted for in the model, since the beam footprint moves over the clear apertures of the optics with field, as shown in Figure 7.

3.2 Polarization sensitivity optimization

As mentioned earlier, it is not possible to measure the diattenuation and retardance as a function of position on the optical elements themselves, and therefore it is not possible to use measured data to model this effect. However, it is possible to assign gradients to the optical elements in the model and use an optimization algorithm to modify these gradients to better match the measured data. The result of such an optimization would indicate only that it is possible that such gradients could explain the sensor-level data, and would not necessarily indicate that the gradients exist as modeled.

The gradients are modeled by applying the scaling functions FRp and FPP to the nominal p-reflectance and retardance (respectively) each optical element. These are planar functions whose independent variables are AOI and surface position, and the dependent variable is either the p-reflectance for FRp or retardance for FPP , as shown in Figure 14. The position coordinate should correspond to the axis of the surface along which the beam moves the most from detector to detector. For the VIIRS FRED model, this axis is always the local y-axis of the surface (as it is for the AFT1 mirror, as shown in Figure 7), and therefore the second independent variable for FRp and FPP will always be the local y-coordinate. The plane used for interpolation is defined by the three points shown in Figure 15 – these points are (min AOI, min y, $FRp0$ or $FPP0$), (max AOI, min y, $FRp1$ or $FPP1$), and (min AOI, max y, $FRp2$ or $FPP2$). The values of min and max AOI and y are computed using the raytracing model. Though both the diattenuation and retardance scaling functions both vary with AOI and position, they are defined with different values for the scaling factors ($FRp0$ vs. $FPP0$, etc.) and therefore have different planar coefficients.

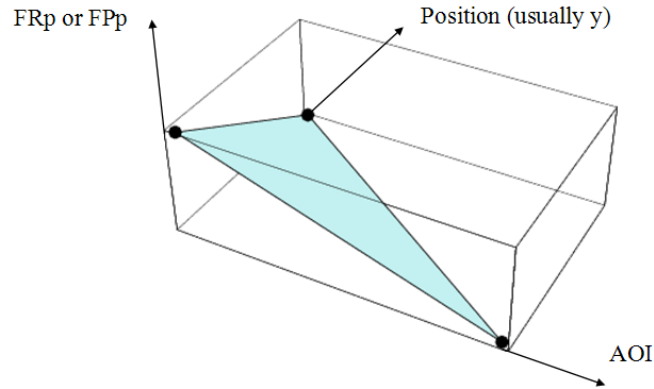


Figure 14. Planar scaling function for diattenuation (FRp) and retardance (FPP). The planes are defined using the points at (min AOI, min y), (max AOI, min y), and (min AOI, max y).

FRp and FPP are applied to the nominal diattenuation D and retardance Δ as:

$$D_{scaled} = D_{nominal} \mp \left[\frac{2R_s}{(R_s + R_p)^2} \right] FRp \quad (2)$$

$$\Delta_{scaled} = \Delta + FPP \quad (3)$$

The term in square brackets in Eq. 2 is the analytic derivative of D with respect to R_p . For highly reflective optics, such as the VIIRS mirrors, $R_p \sim R_s \sim 1$, and therefore $D_{scaled} \sim D_{nominal} \mp FRp$. FRp and FPP are constrained to vary within small values ($-1\% < FRp < 1\%$ and $-10^\circ < FPP < 10^\circ$), though Denton claims that these values are larger than expected. The merit function f used to optimize FRp and FPP for each surface is defined by

$$f = \sqrt{\sum_{i=1}^3 \sum_{j=1}^3 (DoLP_{measured,i,j} - DoLP_{predicted,i,j})^2} \quad (4)$$

where

$DoLP_{measured,i,j}$ is the DoLP measured in STR-554 for the i th detector and the j th scan angle,
 $DoLP_{predicted,i,j}$ is the DoLP predicted for the i th detector and the j th scan angle,
 $i=0$ is detector 0, $i=1$ is detector 8, and $i=2$ is detector 16,
 $j=0$ is scan angle=-45, $j=1$ is scan angle=-8, and $j=2$ is scan angle=+45

Thus f is equal to the RSS difference between the measured and the predicted DoLP at the detectors and scan angles of interest. f is not proportional to the differences in DoLP for all 16 detectors because the goal of this optimization to only roughly match the field variation in DoLP, and not match every peak and valley in the field variation. Such matching would probably require the use of quadratic or higher-order polynomial scaling functions, which is beyond the scope of this effort. The same can be said for the variation in scan mirror angle – only the end and middle points in the scan mirror range are optimized. Powell's quadratically convergent method⁶ was used to minimize the merit function.

To limit the number of optimization variables, it was necessary to first perform a sensitivity analysis by changing the values of $FRpi$ and $FPPi$ ($i=0,1$, or 2) for different surfaces and determining the corresponding change in the merit function. The surfaces which produce the largest change in the merit function will be the ones used in the optimization, and the others will not be used. Doing this neglects any changes in parameter sensitivity that may occur as the optimization proceeds, and thus some parameters that are little help in the beginning of the optimization but would be more help later in the optimization are never used. The result of the sensitivity analysis found that the merit function was most sensitive to changes in diattenuation vs. position (FRp) for the AFT1-AFT4 mirrors. This is consistent with the fact that the beam undergoes a large shift on these elements from one side of the field to the other, as shown in Figure 7 for AFT1. The merit function was least sensitive to changes in retardance vs. position for the AFT1-AFT4 mirrors, and

therefore the FPP parameters were left out of the optimization for these elements. In all, 38 of the 60 parameters (3 points/scaling function x 2 scaling functions/surface x 10 surfaces) were identified as significant performance drivers, and these were the parameters used in the optimization. All bands were found to have similar sensitivities.

4. RESULTS

The results of the optimization are shown in Figures 15-16. Only bands M2, M3, M4, and M6 were optimized. The optimized results agree with the measured results to within 0.5% in DoLP. In most cases, the values of FRp and FPP were optimized to their maximum values ($-1\% < FRp < 1\%$ and $-10^\circ < FPP < 10^\circ$). Figure 17 shows that the variation in DoLP over the field was achieved using the gradients over the AFT optical elements with the sensitivity analysis discussed earlier.

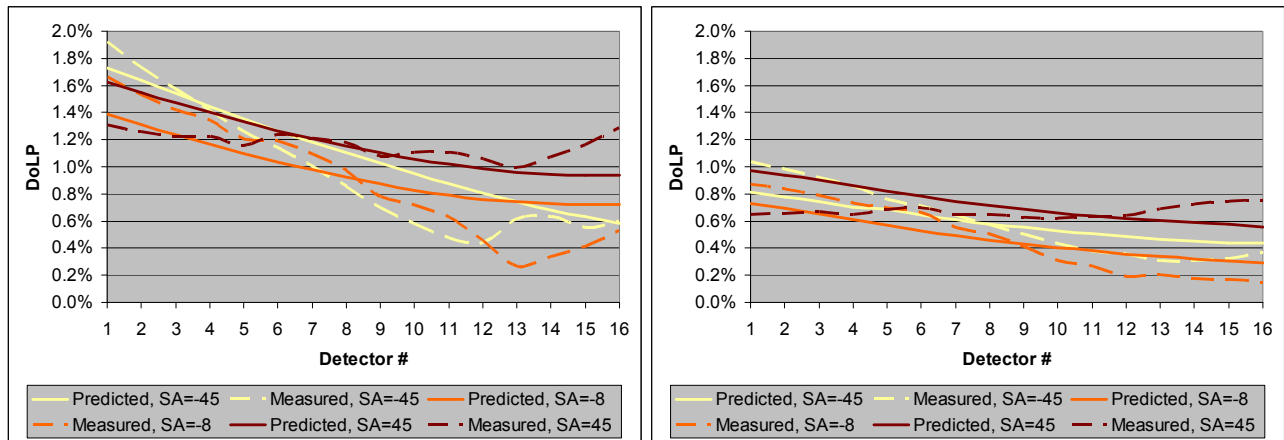


Figure 15. Band M2 (left) and M3 (left) optimized predicted and measured linear polarization sensitivity (DoLP).

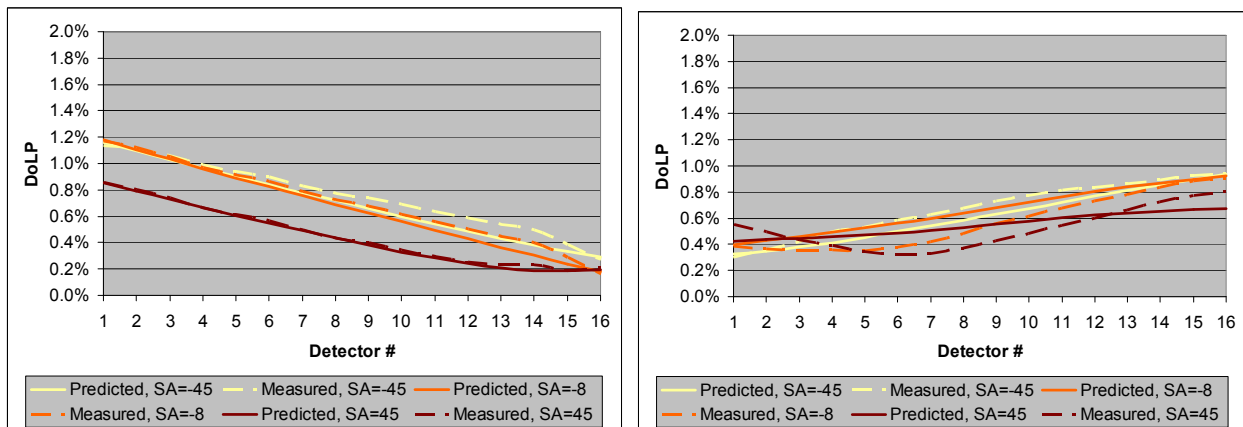


Figure 16. Band M4 (left) and M6 (right) optimized predicted and measured linear polarization sensitivity (DoLP).

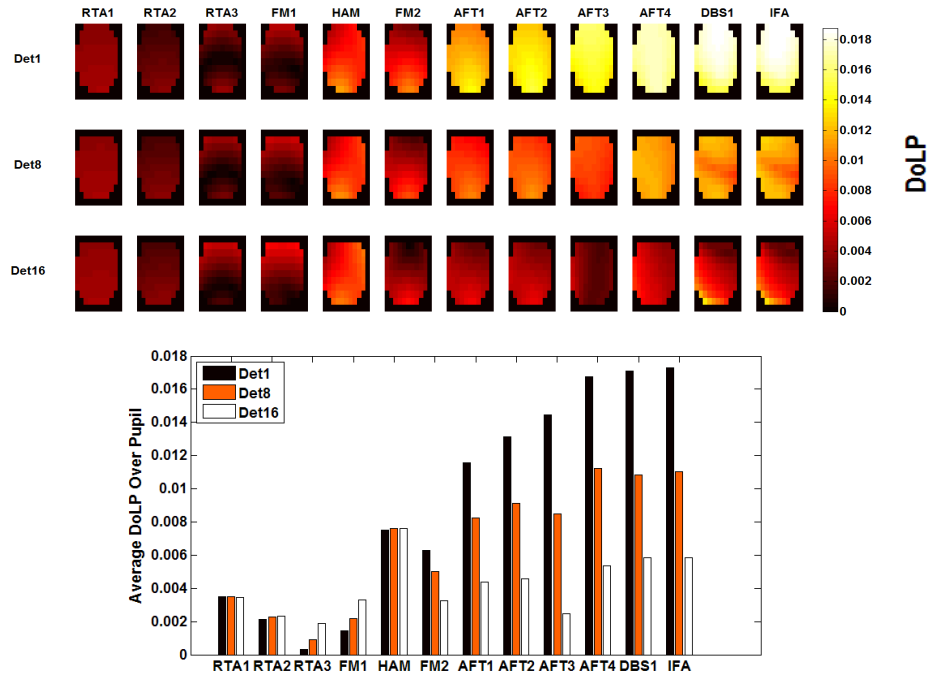


Figure 17. Optimized predicted DoLP vs. pupil position and detector # for band M2, scan angle=-45 (top) and the pupil-averaged DoLP for the same (bottom).

5. CONCLUSIONS

Using measured ellipsometric data, a raytracing model of the VIIRS polarization sensitivity has been constructed. The model demonstrates the expected asymmetry in pupil, scan angle, and field. It also shows weak dependence on mirror diattenuation for the M5 band and strong dependence on scan mirror angle, as expected. The model disagrees with sensor-level polarization sensitivity tests by as much as 1.2% in DoLP, and underestimates the variation in DoLP vs. field angle, especially for bands M2-M4. Spatial gradients of $\pm 1\%$ can be applied to the diattenuation and $\pm 10^\circ$ to the retardance of the optical elements to get better agreement ($\leq 0.5\%$ in DoLP) with the measured DoLP, though these gradients are larger than the spatial variations predicted by the mirror coating manufacturer (Denton). It is not possible to determine the true magnitude of these gradients because it is not possible to perform ellipsometric measurements vs. position on the optical elements. This analysis neglected flux modulation phase, which is equal to the field variation in the phase of the modulation resulting from the linear polarization sensitivity test, and is an important parameter in characterizing the sensor performance. This analysis will be addressed in a future publication.

REFERENCES

- [1] Gordon, H. R., Du, T., and Zhang, T., "Atmospheric correction of ocean color sensors: analysis of the effects of residual instrument polarization sensitivity", *Applied Optics* Vol. 36, No. 27, 6938-6948 (1997)
- [2] Chipman, R., *Handbook of Optics Volume II, Second Ed.*, Optical Society of America, Chapter 22 (1994)
- [3] Stevenson, I. C. and Sadkhin, G., "X-1 silver: a high durability silver coating for use in harsh environments", *Proc. Society of Vacuum Coaters* ISSN 0737-5921 (2000)
- [4] Waluschka, E., Voss, K., Moyer, D., Meister, G., and Liao, L., "VIIRS ZEMAX and FORTRAN polarization models", *Proc. SPIE* 6677 (2007)
- [5] Baumeister, P. W., *Optical Coating Technology*, SPIE Press, 2-33 – 2-34 (2004).
- [6] Press, W. H., Teukolsky, S. A., Vetterling, W. T., and Flannery, B. P., *Numerical Recipes in C, 2nd Ed.*, Cambridge University Press, 1992, 412-420 (1992)